The Astrophysical Journal, 986:200 (6pp), 2025 June 20 https://doi.org/10.3847/1538-4357/add71d

Detection of Hydrocarbons in the Disk around an Actively Accreting Planetary-mass Object

Laura Flagg[1], Aleks Scholz[2], V. Almendros-Abad[3], Ray Jayawardhana[1], Belinda Damian[2], Koraljka Mužić[4], Antonella Natta[5], Paola Pinilla[6], and Leonardo Testi[7]
[1] Department of Physics & Astronomy, Johns Hopkins University, Baltimore, MD 21218, USA; laura.s.flagg@gmail.com
[2] SUPA, School of Physics & Astronomy, University of St. Andrews, North Haugh, St. Andrews, KY16 9SS, UK
[3] Istituto Nazionale di Astrofisica (INAF)—Osservatorio Astronomico di Palermo, Piazza del Parlamento 1, 90134, Palermo, Italy
[4] Instituto de Astrofísica e Ciências do Espaço, Faculdade de Ciências, Universidade de Lisboa, Ed. C8, Campo Grande, 1749-016 Lisbon, Portugal
[5] School of Cosmic Physics, Dublin Institute for Advanced Studies, 31 Fitzwilliam Place, Dublin 2, Ireland
[6] Mullard Space Science Laboratory, University College London, Holmbury St. Mary, Dorking, London, UK
[7] Dipartimento di Fisica e Astronomia, Università di Bologna, Via Gobetti 93/2, 40122, Bologna, Italy
Received 2025 February 9; revised 2025 April 30; accepted 2025 May 5; published 2025 June 18

Abstract

We present the 0.6–12 μm spectrum of Cha 1107-7626, a 6–10 Jupiter-mass free-floating object in the ∼2 Myr-old Chamaeleon-I star-forming region, from observations with the NIRSpec and MIRI instruments on board the James Webb Space Telescope. We confirm that Cha 1107-7626 is one of the lowest-mass objects known to harbor a dusty disk with infrared excess emission at wavelengths beyond 4 μm. Our NIRSpec data and prior ground-based observations provide strong evidence for ongoing accretion through hydrogen recombination lines. In the mid-infrared spectrum, we detect unambiguously emission lines caused by methane (CH_4) and ethylene (C_2H_4) in its circumsubstellar disk. Our findings mean that Cha 1107-7626 is by far the lowest-mass object with hydrocarbons observed in its disk. The spectrum of the disk looks remarkably similar to that of ISO-ChaI 147, a very low-mass star with a carbon-rich disk that is 10–20 times more massive than Cha 1107-7626. The hydrocarbon lines can be accounted for with a model assuming gas temperatures of a few hundred kelvin in the inner disk. The obvious similarities between the spectra of a low-mass star and a planetary-mass object indicate that the conditions in the inner disks can be similar across a wide range of central object masses.

Unified Astronomy Thesaurus concepts: Brown dwarfs (185); Stellar accretion (1578); Protoplanetary disks (1300); Free floating planets (549); Infrared spectroscopy (2285); Stellar accretion disks (1579)

Materials only available in the online version of record: data behind figure

1. Introduction

Planets are born in disks around young stars. These protoplanetary disks have been identified for central objects across the entire range of stellar and substellar masses, including some that have masses comparable to giant planets (A. Natta & L. Testi 2001; R. Jayawardhana et al. 2003a; K. L. Luhman et al. 2006). Until very recently, most of the work on substellar disks has been focused on the dust component, by necessity, since its thermal emission is straightforward to detect as infrared excess. The suite of instruments on board the James Webb Space Telescope (JWST; J. Rigby et al. 2023) now provide us with an excellent opportunity to study the gas in the inner disks of young stars and brown dwarfs.

Here we present the first detection of mid-infrared emission lines originating in the inner disk around a young free-floating planetary-mass object. Our target, Cha 1107-7626, has an estimated mass of 6–10 $M_{\rm Jup}$, and is one of the lowest mass objects known to have infrared excess emission from a circumsubstellar disk as well as evidence of gas accretion (K. L. Luhman et al. 2008; V. Almendros-Abad et al. 2022). In the JWST/MIRI spectrum, we find strong emission from the hydrocarbons methane and ethylene, molecules that have previously been identified in disks around stars down to masses of ∼0.1 $M_\odot$ (B. Tabone et al. 2023; A. M. Arabhavi et al. 2024). Thus, for the first time, we have the opportunity to probe the physical conditions of the warm molecular gas in a disk around an object with a >10 times lower mass and a >100 times lower luminosity than known so far.

2. Background on Cha 1107-7626

Cha J11070768-7626326 (hereafter Cha 1107-7626) was identified by K. L. Luhman et al. (2008). In the discovery paper, the authors show evidence of infrared excess from Spitzer photometry and of accretion from Hα emission in an optical spectrum. A recent compilation of young brown dwarf spectra by V. Almendros-Abad et al. (2022) included a near-infrared Very Large Telescope/SINFONI spectrum of our target, with a resolution of 1500–2000.

K. L. Luhman et al. (2008) classified the object as L0 ± 1, with $T_{\rm eff}$ of 2200 K and a bolometric luminosity of 3.3×10^{-4} $L_\odot$. Based on those figures, they estimated a mass of 0.004–0.01 $M_\odot$. In this paper, we confirm and refine the estimates for the substellar parameters.

The object is located in the northern part of the 1–3 Myr old Chamaeleon-I star-forming region. According to the most recent estimates based on Gaia DR2, this region is at ∼190 pc (V. Almendros-Abad et al. 2024), but earlier studies typically adopted a distance closer by 20–30 pc (V. Roccatagliata et al. 2018).

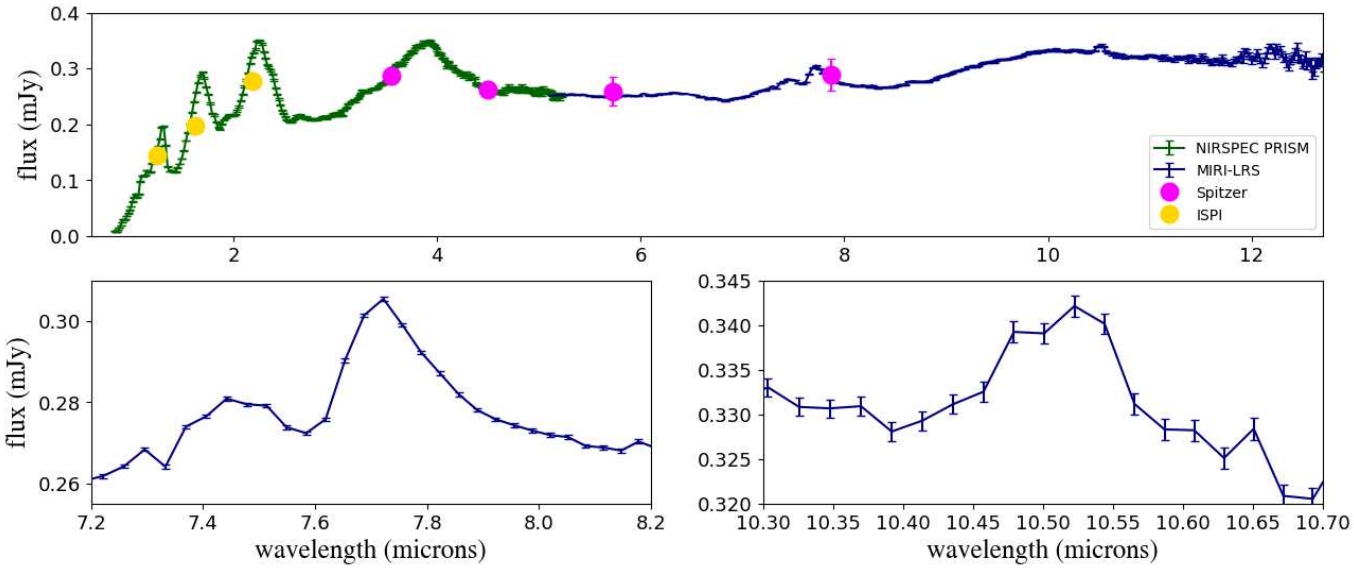

Figure 1. Top: the JWST spectrum of Cha 1107-7626 taken with NIRSpec-PRISM (green) and MIRI-LRS (blue). Overplotted are the ISPI and Spitzer photometric points from K. L. Luhman et al. (2008). Bottom: the spectral data plotted above, zoomed-in on two spectral features in the mid-infrared, which we identify as methane and ethylene (see Section 5).

3. Observation and Data

We observed Cha 1107-7626 with JWST on 2024 August 21 using NIRSpec-PRISM and MIRI-LRS (low-resolution spectrometer); see MAST doi:10.17909/jnt4-qg74. The instruments achieve a resolution of $R \sim 100$. These observations were part of the GO cycle 3 program 4583 (PI: A. Scholz). The JWST spectra were reduced with pipeline version 1.15.1 (H. Bushouse et al. 2024) using the default settings with the exception that we chose to use *pixel_replace*. The NIRSpec and MIRI spectra match each other at a wavelength of 5 μm; they also match the available photometry within the errorbars, indicating that the calibration is robust. The errorbars are directly from the pipeline, and thus only include random noise and not the several percent uncertainty in absolute flux calibration. We removed outliers that differed by more than 5% from both neighboring points and replaced those values with the average of the two neighboring pixels; this only affected two data points at wavelengths short of 12 μm. The full dataset is shown in Figure 1. In the near-infrared, the spectrum shows the molecular absorption bands typical of young late-type objects. In the mid-infrared, the spectrum is flat within ±20% with notable emission features at 7.7 and 10.5 μm at signal-to-noise ratios of 90 and 13.8 above the continuum, respectively. We show plots zoomed-in on those features in the bottom half of Figure 1. We note that the spectrum is affected by excessive noise beyond $\lambda = 12\,\mu$m. We do not use this part of the spectrum in the following. As seen in Figure 1, there may be another spectral feature between 12 and 12.5 μm (see Section 5.1). An emission spike at 12.8 μm is the result of a single pixel with excess flux in only one of the two dithers; we thus believe it is caused by cosmic-ray contamination.

4. The Central Object

4.1. Basic Parameters

We remeasured the spectral type (SpT) using the NIRSpec data by comparing with spectral templates of young objects. We followed a procedure very similar to that of A. B. Langeveld et al. (2024). In short, we fit a set of templates to our spectrum, with SpT and extinction as free parameters, normalizing the template at a wavelength of 1.66 μm. Here we use the extinction law by S. Wang & X. Chen (2019). We find that templates in the M9-L1 range provide a good fit (see Figure 2, top), confirming the previously determined SpT. The extinction for these types would be $A_V = 0.4$–2.8 mag.

We also compare BT-Settl models (F. Allard et al. 2012) to the NIRSpec spectrum between 0.7 and 4.0 μm. A model with $T_{\rm eff} = 1900 \pm 100$ K, $\log g = 3.5$, and reddened by $A_V \sim 1$ mag provides a good match and minimizes the χ^2. In general, the model spectra for 1800–2000 K fit well (Figure 2, bottom), with the exception of the peak at ∼4 μm. The comparison also reveals the presence of significant excess emission above the photosphere for wavelengths beyond 4 μm.

With an apparent J-band magnitude of 17.61, extinction of $A_V = 1$, and a distance of 190 pc, the absolute magnitude is $M_J = 10.97$. Comparing the temperature and absolute magnitude to the ATMO2020 model isochrones (M. W. Phillips et al. 2020) with ages of 1–5 Myr yields a mass between 6 and 10 Jupiter masses, again in agreement with previous estimates. Our findings on the object are summarized in Table 1.

4.2. Accretion Rate

The available ground-based optical (K. L. Luhman et al. 2008) and infrared (V. Almendros-Abad et al. 2022) spectra show strong Hα and Paβ emission, both clear signs of accretion (C. F. Manara et al. 2017). The Hα emission has a 10% full width of 374 km s^{-1}, well over the typical 200 km s^{-1} accretion cutoff in brown dwarfs (R. Jayawardhana et al. 2003b). The Hα line is also visible in our new NIRSpec data, albeit at much lower resolution. Here, we derive the mass accretion rates from these lines. We flux calibrated the optical spectrum from K. L. Luhman et al. (2008) by comparing it to the NIRSpec spectrum for $\lambda < 850$ nm, avoiding regions of strong telluric absorption and the Hα line itself. The available

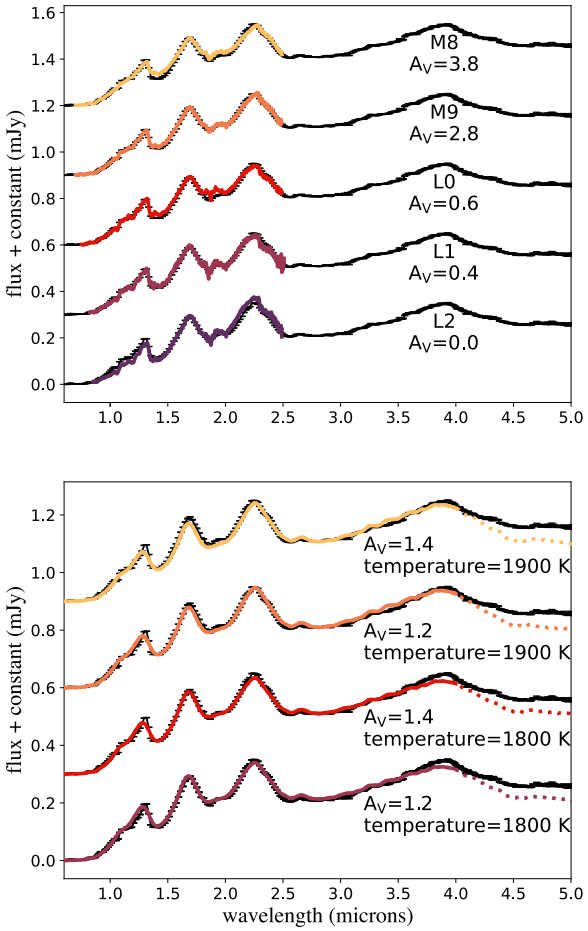

Figure 2. Top: empirical spectral templates in comparison with the NIRSpec data. Templates between M9 and L1 match our data best. At earlier SpTs ($\leqslant$M8.5), the slope of the H band between 1.5 and 1.8 μm is too flat, indicating that the source is a later type. Whereas at later SpTs ($\geqslant$L2), the templates overestimate the flux in the J band, presenting an overall worse fit than in the M9-L1 range. Bottom: BT-Settl model spectra matched to the NIRSpec data. Models with $T_{\rm eff}$ between 1800 and 2000 K provide a good fit to the data.

SINFONI spectrum is flux calibrated by comparison with JHK photometry (V. Almendros-Abad et al. 2022). We show the hydrogen emission lines in Figure 3.

We estimate the Hα and Paβ line fluxes from the published spectra with the same method used in V. Almendros-Abad et al. (2024). We converted to line luminosities using a distance of 190 pc. To derive accretion luminosities, we used the J. M. Alcalá et al. (2017) relationships. In these steps, all uncertainties are propagated through. We derived accretion luminosities of $\log L_{\rm acc} = -3.8 \pm 0.6\, L_\odot$ from Paβ and $-4.6 \pm 0.3\, L_\odot$ from Hα. Lastly, we estimated the mass accretion rate assuming a truncation radius of $5R_*$ and an object radius of 0.21 $R_\odot$, using $\dot{M}_{\rm acc} = 1.25 \cdot L_{\rm acc} R_*/(GM_*)$. We find $\log \dot{M}_{\rm acc} = -9.7 \pm 0.8\, M_\odot\,{\rm yr}^{-1}$ using Paβ, and $-10.6 \pm 0.4\, M_\odot\,{\rm yr}^{-1}$ using Hα. The Paβ accretion estimate is larger than using Hα, but the two values are consistent with each other within the errors.

As far as we are aware, Cha 1107-7626 is the lowest mass isolated object with confirmed gas accretion observed in optical and near-infrared emission lines. Measurements of accretion rates in sources of similar mass (SpT $\geqslant$ M9) are typically $\leqslant 10^{-10}$–$10^{-10.5}\, M_\odot\,{\rm yr}^{-1}$ (S. Mohanty et al. 2005; G. J. Herczeg & L. A. Hillenbrand 2008; V. Joergens et al. 2013; S. Petrus et al. 2020; V. Almendros-Abad et al. 2024). Similarly, G. Viswanath et al. (2024) report an accretion rate of $1.4 \cdot 10^{-11}\, M_\odot\,{\rm yr}^{-1}$ for a young L2 brown dwarf with a mass straddling the deuterium-burning limit.

Table 1
The Physical Parameters Measured for the Cha 1107-7626 System

Parameter	Value
Mass	6–10 $M_{\rm Jup}$
Effective Temperature	1900 $\pm$ 100 K
Spectral Type	L0 $\pm$ 1
V-band Extinction	$\sim$1 mag
Log Accretion Luminosity	$-4.6 \pm 0.3\, L_\odot$
Log Accretion Rate Paβ	-9.7 log ($M_\odot\,{\rm yr}^{-1}$)
Log Accretion Rate Hα	-10.6 log ($M_\odot\,{\rm yr}^{-1}$)

Compared to these values, our target is quite strongly accreting for its mass, and this is especially significant in the case of the measurement derived from Paβ (Figure 4). A similar case may be OTS 44, a M9.5 member of Cha-I. V. Joergens et al. (2013) estimated accretion rates of OTS 44 and find that the value from Paβ is about 2 orders of magnitudes larger than the one from Hα. They concluded that Paβ emission may have an origin different from accretion, but do not specify an alternative. The measurements OTS 44 and Cha 1107-7626 may indicate that the empirical methodology to determine accretion rates may need to be reconsidered for the planetary-mass domain.

Recently, J. Hashimoto & Y. Aoyama (2025) have found that the hydrogen lines of a nonnegligible fraction of free-floating substellar objects are better reproduced by "accretion shock" models, rather than "accretion flow" models developed for accreting stars. Y. Aoyama et al. (2021) developed relationships between line and accretion luminosities in the context of an "accretion-shock" model. Using these relations, we estimate a mass accretion rate $\log \dot{M}_{\rm acc} = -9.1 \pm 0.3\, M_\odot\,{\rm yr}^{-1}$ using Paβ, and $-9.7 \pm 0.3\, M_\odot\,{\rm yr}^{-1}$ using Hα. Thus, these models predict an accretion rate 0.6–0.9 dex larger than from the conventional procedure and would make it even more discrepant from the trends found in the stellar regime.

5. The Disk Emission

5.1. Overview

In Figure 5, upper panel, we show our MIRI mid-infrared spectrum for Cha 1107-7626 (black) in comparison with a photospheric model (bright blue, see Section 4.1). As can be appreciated from this figure, the object shows substantial excess emission in the infrared, indicating the presence of a disk. At wavelengths $>8\,\mu$m, the emission from the disk dominates over the photosphere.

The MIRI spectrum also shows two notable spectral features at approximately 7.7 and 10.5 μm (highlighted in Figure 1). Compared with the literature on molecular emission in disks around young stars, these features can be clearly identified as methane (CH_4) and ethylene (C_2H_4) emission from the disk (A. M. Arabhavi et al. 2024). There is a hint of emission at 12–12.5 μm that could be due to C_2H_6 (ethane), but the low signal-to-noise prevents a definitive detection at this time. We see no evidence of CO, H_2O, or C_2H_2.

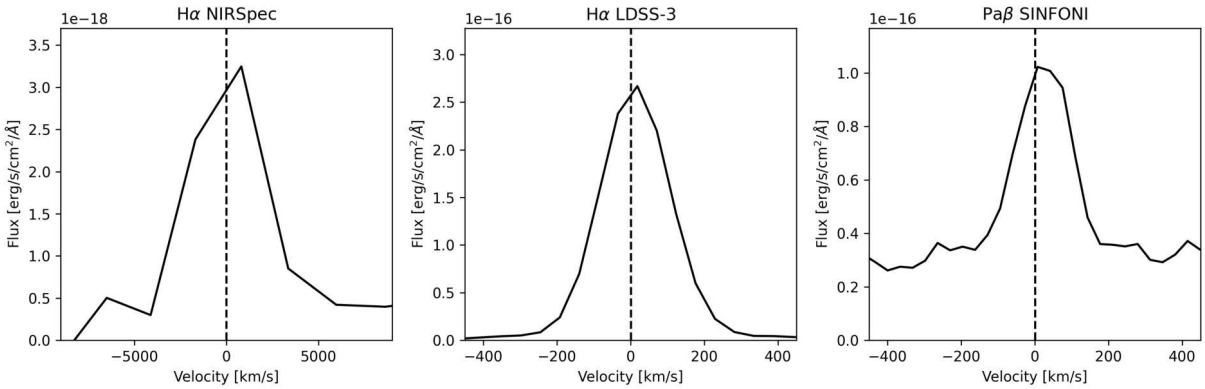

Figure 3. Zoom to the region around the Hα and Paβ emission lines in our NIRSpec data, as well as the LDSS-3 and SINFONI spectra of Cha 1107-7626, respectively. Note that in the NIRSpec data, the width of the line is due to the low-resolution of the instrument. Originally the spectra in the middle and right panel were published in K. L. Luhman et al. (2008) and V. Almendros-Abad et al. (2022).

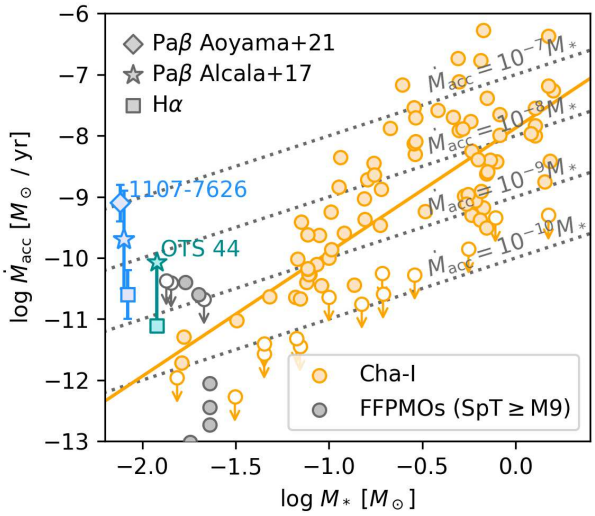

Figure 4. Relationship between M_* and $\dot{M}_{acc}$ for Cha 1107-7626 (blue symbols; this work), OTS 44 (cyan symbols; V. Joergens et al. 2013), remaining Cha-I members with accretion estimate available (orange circles; C. F. Manara et al. 2023; V. Almendros-Abad et al. 2024), and other FFPMOs (S. K. Betti et al. 2023; V. Almendros-Abad et al. 2024). The solid orange line represents the correlation between these parameters found for Cha-I members in V. Almendros-Abad et al. (2024). Cha 1107-7626 has an unusually high accretion rate given its mass in comparison with other low-mass stars and brown dwarfs. Additionally, the rate measured from Paβ is higher than that from Hα.

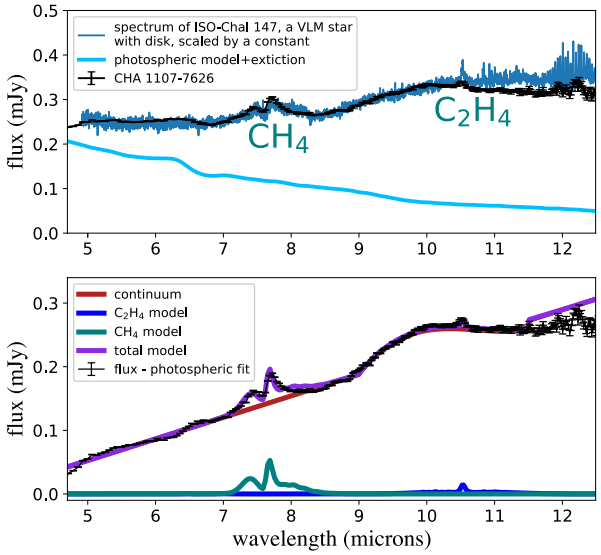

Figure 5. Top: the JWST spectrum of Cha 1107-7626 (black), its best-fit photospheric model (light blue), corrected for extinction. In blue we overplot the MIRI-MRS spectrum of ISO-ChaI 147, scaled by a constant. Bottom: The MIRI spectrum minus the best-fit photosphere (black), and the best-fit models for the continuum (dark red), CH_4 (green), and C_2H_4 (blue). Also plotted is the sum of those models (purple). Data from this figure is available as data behind the figure.

(The data used to create this figure are available in the online article.)

In Figure 5 we also show the MIRI/MRS spectrum of ISO-ChaI 147 published by A. M. Arabhavi et al. (2024), scaled by a constant factor chosen to match the flux levels in our spectrum for Cha 1107-7626. ISO-ChaI 147 also shows the same two emission features in its mid-infrared spectrum. ISO-ChaI 147 is a classical T Tauri star with a mass of 0.11 $M_\odot$ (I. Pascucci et al. 2016), about 10–20 times more massive than our target, and about 2 orders of magnitude more luminous. Despite these differences, the spectra match remarkably well, both in the continuum and in the emission features. This illustrates that structure and chemical evolution of the inner disks can be self-similar, across a wide range of central object masses.

5.2. Modeling the Gas Disk Emission

To further analyze the molecular emission features, we used *slabspec* (C. Salyk 2022) to create LTE slab models of CH_4 and C_2H_4 that would reproduce the excess emission, i.e., the data minus the best-fit photospheric model. To remove the disk continuum around the methane feature, we matched the spectrum from 5.5 to 7.0 μm and from 8.5 to 9.0 μm with a linear function. Around the ethylene feature, we subtracted a third-order polynomial fit to remove the continuum, which may be contaminated by silicate emission (see the analysis in B. Damian et al. 2025, in preparation). The fit for the continuum is shown in Figure 5, bottom panel, in red.

Our model slab spectra were created with a grid ranging in column densities from 10^{16} to 10^{20} cm^{-2}, in temperatures from 100 to 1300 K, and emitting areas from 10^{20} to 10^{23} cm^2. We used all isotopes with available line lists and fixed the relative abundances for those isotopes to the ratios from HITRAN (I. E. Gordon et al. 2022). We then convolved the models with a Gaussian to match the approximate resolution of each

section. For each model, we calculate the reduced χ^2, designated as χ^2_ν (P. R. Bevington & D. K. Robinson 2003). The best-fitting models are obtained for a gas temperature of a few hundred kelvin. An example of the outcomes of the comparison with the slab models is shown in Figure 5, lower panel.

Our modeling conclusively demonstrates that the features we see are indeed CH_4 and C_2H_4, as shown in Figure 5. However, the match between observed features and models is poor with regard to χ^2_ν. There are several potential reasons for the mismatch. First, we know for certain that the uncertainties we use underrepresent the true uncertainty (see Section 3). We also assume a single temperature slab and a simple nonphysical model for the continuum flux. Finally, there could be other species with opacities at the relevant wavelengths that are contributing to the spectral features we see. For example, the CH_4 emission is known to be blended with a C_2H_2 feature. For these reasons, we cannot put stringent constraints on the physical properties of the gas.

6. Discussion and Summary

In this paper, we show a complete infrared spectrum from 1 to 12 μm for Cha 1107-7626, a young free-floating planetary-mass object in the Chamaeleon-I star-forming region (K. L. Luhman et al. 2008). Using our new data, we rederive the properties of the object, and estimate a temperature of $\sim$1900 K and a mass of 6–10 Jupiter masses. In previously published spectra, as well as our JWST data, the object shows clear hydrogen recombination emission lines indicating ongoing accretion. We estimate an accretion rate of 10^{-10}–10^{-11} solar masses per year, comparable to higher mass brown dwarfs. This is the lowest mass isolated object with confirmed accretion in multiple lines in the optical and infrared. The accretion luminosity is $\sim$8% of the bolometric luminosity.

In the mid-infrared, Cha 1107-7626 exhibits two obvious emission line features at 7.7 and 10.5 μm, which we attribute to emission from methane and ethylene, respectively. There is a hint of possible ethane emission at 12–12.5 μm. Based on a comparison with slab models, we find that the temperature of the molecular gas that is causing these lines is likely to be in the range of a few hundred kelvin. With only two lines, these constraints are not very restrictive, but they are reasonable in comparison with more extensive modeling for hydrocarbon lines seen in disks around more massive stars.

The emission line features present in the infrared spectrum of Cha 1107-7626 present us with an opportunity to study gas accretion and the physical conditions in the warm inner gaseous disk in depth, for the first time for an object with a mass below 10 times the mass of Jupiter. This makes Cha 1107-7626 a compelling target for follow-up observations.

The mid-infrared spectra of disks around young stars display great variety, implying substantial diversity in the underlying physical conditions. The presence of hydrocarbons is indicative of a carbon-rich chemistry and a high C/O ratio in the gas phase (J. Kanwar et al. 2024). The hydrocarbon features discussed seem to be common in disks around very low-mass stars (I. Pascucci et al. 2013; B. Tabone et al. 2023; A. M. Arabhavi et al. 2024; A. M. Arabhavi et al. 2025), including one with an age of 30 Myr (F. Long et al. 2025). Similarly, the lack of oxygen-bearing gas species is indicative of a high C/O ratio and a low oxygen abundance in the gaseous component of the disk, similar to what is seen in disks around very low-mass stars (e.g., B. Tabone et al. 2023; A. M. Arabhavi et al. 2024).

The mid-infrared spectrum for Cha 1107-7626 looks remarkably similar to that of ISO-ChaI 147, a very low-mass star in the same star-forming region (Figure 5). Both the continuum and the emission lines in the spectrum of Cha 1107-7626 are well reproduced by simply scaling the spectrum for ISO-ChaI 147 by a constant factor. These comparisons indicate that disk evolution processes and disk chemistry are similar across a wide range of stellar/substellar masses and luminosities.

Numerous studies focused on the dust component have stressed that brown dwarf disks evolve following an overall phenomenology that is comparable to disks around stars (K. L. Luhman 2012). With our new findings, we begin to see that the same may apply to the gas in the inner parts of the disks. Disks around planetary-mass objects, with masses less than 1% the mass of the Sun, can harbor the same array of molecular line emission that JWST observations have recently revealed in disks around low-mass stars. In particular, our object shows clear signs of a carbon-rich chemistry. This is a further indication that the evolutionary processes in disks are robust across several orders of magnitude in mass. The disk of Cha 1107-7626 may present us with clues that isolated planetary-mass objects can form their own retinues, raising the prospect of miniature planetary systems in their midst.

Acknowledgments

We would like to thank our anonymous referee for their helpful comments. We thank Kevin Luhman who made his optical spectrum available to us. L.F. and R.J. acknowledge support for the JWST-GO-04583.008 program provided by NASA through a grant from the Space Telescope Science Institute, which is operated by the Association of Universities for Research in Astronomy, Inc., under NASA contract NAS 5-03127. A.S. and B.D. acknowledge support from the UKRI Science and Technology Facilities Council through grant ST/Y001419/1/. K.M. acknowledges support from the Fundação para a Ciência e a Tecnologia (FCT) through the CEEC-individual contract 2022.03809.CEECIND and research grants UIDB/04434/2020 and UIDP/04434/2020.

ORCID iDs

Laura Flagg https://orcid.org/0000-0001-6362-0571
Aleks Scholz https://orcid.org/0000-0001-8993-5053
V. Almendros-Abad https://orcid.org/0000-0002-4945-9483
Ray Jayawardhana https://orcid.org/0000-0001-5349-6853
Belinda Damian https://orcid.org/0000-0002-2234-4678
Koraljka Mužić https://orcid.org/0000-0002-7989-2595
Antonella Natta https://orcid.org/0000-0002-4608-7995
Paola Pinilla https://orcid.org/0000-0001-8764-1780
Leonardo Testi https://orcid.org/0000-0003-1859-3070

References

Alcalá, J. M., Manara, C. F., Natta, A., et al. 2017, A&A, 600, A20
Allard, F., Homeier, D., Freytag, B., & Sharp, C. M. 2012, in EAS Pub. Ser. 57, Low-Mass Stars and the Transition Stars/Brown Dwarfs, ed. C. Reylé, C. Charbonnel, & M. Schultheis (Les Ulis: EDP Sciences), 3
Almendros-Abad, V., Manara, C. F., Testi, L., et al. 2024, A&A, 685, A118
Almendros-Abad, V., Mužić, K., Moitinho, A., Krone-Martins, A., & Kubiak, K. 2022, A&A, 657, A129

Aoyama, Y., Marleau, G.-D., Ikoma, M., & Mordasini, C. 2021, ApJL, 917, L30
Arabhavi, A. M., Kamp, I., Henning, T., et al. 2024, Sci, 384, 1086
Arabhavi, A. M., Kamp, I., van Dishoeck, E. F., et al. 2025, ApJL, 984, L62
Betti, S. K., Follette, K. B., Ward-Duong, K., et al. 2023, AJ, 166, 262
Bevington, P. R., & Robinson, D. K. 2003, Data Reduction and Error Analysis for the Physical Sciences (Boston, MA: McGraw-Hill)
Bushouse, H., Eisenhamer, J., Dencheva, N., et al. 2024, JWST Calibration Pipeline, Version 1.15.1, Zenodo, doi:10.5281/zenodo.12692459
Gordon, I. E., Rothman, L. S., Hargreaves, R. J., et al. 2022, JQSRT, 277, 107949
Hashimoto, J., & Aoyama, Y. 2025, AJ, 169, 93
Herczeg, G. J., & Hillenbrand, L. A. 2008, ApJ, 681, 594
Jayawardhana, R., Ardila, D. R., Stelzer, B., & Haisch, K. E., Jr. 2003a, AJ, 126, 1515
Jayawardhana, R., Mohanty, S., & Basri, G. 2003b, ApJ, 592, 282
Joergens, V., Bonnefoy, M., Liu, Y., et al. 2013, A&A, 558, L7
Kanwar, J., Kamp, I., Jang, H., et al. 2024, A&A, 689, A231
Langeveld, A. B., Scholz, A., Mužić, K., et al. 2024, AJ, 168, 179
Long, F., Pascucci, I., Houge, A., et al. 2025, ApJL, 978, L30
Luhman, K. L. 2012, ARA&A, 50, 65
Luhman, K. L., Allen, L. E., Allen, P. R., et al. 2008, ApJ, 675, 1375
Luhman, K. L., Wilson, J. C., Brandner, W., et al. 2006, ApJ, 649, 894
Manara, C. F., Ansdell, M., Rosotti, G. P., et al. 2023, in ASP Conf. Ser. 534, Protostars and Planets VII, ed. S.-i. Inutsuka (San Francisco, CA: ASP)
Manara, C. F., Frasca, A., Alcalá, J. M., et al. 2017, A&A, 605, A86
Mohanty, S., Jayawardhana, R., & Basri, G. 2005, ApJ, 626, 498
Natta, A., & Testi, L. 2001, A&A, 376, L22
Pascucci, I., Herczeg, G., Carr, J. S., & Bruderer, S. 2013, ApJ, 779, 178
Pascucci, I., Testi, L., Herczeg, G. J., et al. 2016, ApJ, 831, 125
Petrus, S., Bonnefoy, M., Chauvin, G., et al. 2020, A&A, 633, A124
Phillips, M. W., Tremblin, P., Baraffe, I., et al. 2020, A&A, 637, A38
Rigby, J., Perrin, M., McElwain, M., et al. 2023, PASP, 135, 048001
Roccatagliata, V., Sacco, G. G., Franciosini, E., & Randich, S. 2018, A&A, 617, L4
Salyk, C. 2022, Csalyk/Spectools_ir: First Release, Version v1.0.0, Zenodo, doi:10.5281/zenodo.5818682
Tabone, B., Bettoni, G., van Dishoeck, E. F., et al. 2023, NatAs, 7, 805
Viswanath, G., Ringqvist, S. C., Demars, D., et al. 2024, A&A, 691, A64
Wang, S., & Chen, X. 2019, ApJ, 877, 116